Online digital compensation of pump dithering induced phase and amplitude distortions in transmission links with cascaded fibre-optical parametric amplifiers

LONG H. NGUYEN,[1,2] **SONIA BOSCOLO,**[1,3] **AND STYLIANOS SYGLETOS**[1,4]

[1]*Aston Institute of Photonic Technologies, Aston University, Birmingham B4 7ET, United Kingdom*
[2]*lnguy19@aston.ac.uk*
[3]*s.a.boscolo@aston.ac.uk*
[4]*s.sygletos@aston.ac.uk*

Abstract: We present an advanced online digital signal processing (DSP) method for correcting the phase and amplitude distortions caused by the phase modulation of the pump source and its interaction with the dispersive fibre channel in transmission systems using cascaded fibre-optical parametric amplifiers. The proposed algorithm is numerically demonstrated to achieve significant (up to 3.7 dB for a four-tone pump-phase modulation scheme) Q^2-factor performance improvement over conventional DSP in 16 quadrature-amplitude modulation signal transmission.

1.   Introduction

Fibre-optical parametric amplifiers (FOPAs), utilising four-wave mixing (FWM) to amplify the signals, present a number of distinguishing properties that could potentially be exploited to boost the capability of optical communication systems [1]. These include adjustable centre frequency and gain spectrum, facilitating broadband [2] or high-gain [3] amplification at virtually arbitrary wavelengths [4], phase-sensitive amplification [5], and ultra-fast response. Over the past two decades, FOPA research has focused on sub-system and system studies, incorporating a few basic amplifier's features to address engineering challenges in practical optical communication deployments. While significant progress in terms of realising polarisation-insensitive gain and mitigating nonlinear cross-talk has been achieved recently [6], the mitigation of stimulated Brillouin scattering (SBS) remains a primary challenge for FOPAs. The SBS effect limits the pump power that can be delivered to the highly nonlinear fibre (HNLF), and thereby the achievable nonlinear phase shift. A common SBS mitigation strategy relies on broadening the line-width of the pump source to minimise the power spectral density integrated over the Brillouin bandwidth (typically tens of megahertz). This is most often done via external phase modulation of the pump source [7,8], known as phase dithering, using, e.g., a combination of radio-frequency (RF) tones at different frequencies. While pump-phase modulation is a very effective SBS mitigation method [3], it leads to a modulation of the phase-matching conditions because the instantaneous pump frequency is also modulated, and this in turn modulates the gain [9]. This is primarily a source of phase distortion for coherently detected complex-amplitude signals widely used in modern optical communications. The impact of pump dithering on the FOPA performance has been studied for both directly detected on-off keying [10,11] and coherently detected quadrature-amplitude modulation (QAM) [12] signals in a back-to-back optical configuration.

Digital signal processing (DSP) can address performance issues of communication system's components and devices from a different perspective: by reducing the induced signal penalties
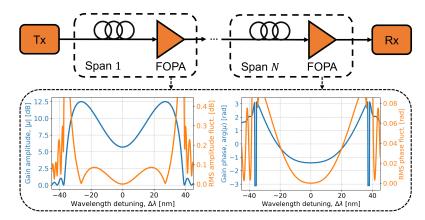
on the receiver side rather than developing more complex device's architectures with improved characteristics. In this context, our recent work has developed a number of advanced DSP techniques that can effectively address the impact of phase distortion caused by pump dithering in fibre-optical parametric devices [13,14]. Having a relatively high frequency (in the gigahertz range), the dithering-induced phase distortion can not be tracked and sufficiently suppressed by the conventional carrier phase recovery (CPR) schemes used in commercial coherent receivers [15–17], which have been designed to operate on the slower (several tens of kilohertz frequency) phase noise induced by non-zero laser spectral width. Furthermore, the interaction of this intrinsic dithering-induced phase distortion with the chromatic dispersion of the fibre in a transmission link results in a phase-to-amplitude distortion transfer [18], which becomes more severe with increasing transmission distance along the link because of the extended channel memory. In [14], we presented a scheme to mitigate the dithering-induced phase distortion and its conversion into amplitude distortion in transmission links using mid-span optical phase conjugation.

This paper expands upon the approach of [14] by applying it to transmission links with cascaded in-line FOPAs, operating with multi-tone pump-phase modulation to support sufficient SBS-limited gain [3]. We introduce a novel, fully online DSP scheme enabling the removal of the accumulated phase and amplitude distortions that have been independently contributed by each FOPA stage in the link. The technique is numerically demonstrated in 28-Gbaud 16-QAM FOPA-assisted transmission, achieving up to 3.7-dB Q^2-factor improvement over conventional DSP.

2. Methods

2.1. Transmission link and FOPA model

We considered an optical fibre transmission system comprising N identical spans, each of 100-km standard single-mode fibre (dispersion parameter $D = 17\,\text{ps/(nm} \cdot \text{km)}$, nonlinear coefficient $\gamma' = 1.2\,(\text{W} \cdot \text{km})^{-1}$, loss coefficient $\alpha = 0.2$ dB/km) followed by a FOPA to compensate the span losses, as shown in Fig. 1.
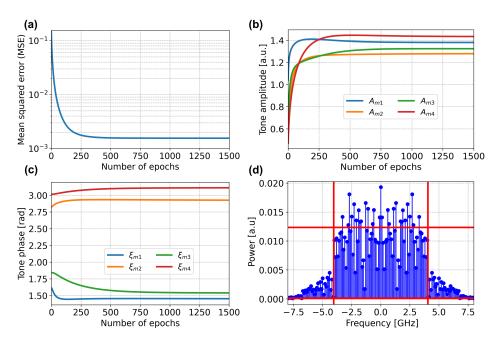

Fig. 1. Schematic diagram of a transmission system with N cascaded FOPA stages. The inset shows the amplitude and phase spectral responses of the FOPA's parametric gain versus the detuning from the pump and the respective dithering-induced RMS fluctuations, as obtained from Eq. (1).

Our FOPA model adopted a single-pump design and calculated the signal gain in the absence of pump depletion as [9,19]

$$\mu = \{\cosh(gL) + i\,[(\kappa + \delta\kappa)/(2g)]\sinh(gL)\}\,e^{i[2\gamma P - (\kappa + \delta\kappa)/2]L}, \tag{1}$$

where P is the pump power, L is the effective fibre length, $g = \sqrt{(\gamma P)^2 - (\kappa + \delta\kappa)^2/4}$ is the parametric gain coefficient, $\kappa = 2\gamma P + \beta_2\Omega^2 + (\beta_4/12)\Omega^4$ is the standard phase mismatch, $\delta\kappa(t) = \beta_2\varphi_t^2 - \beta_3(\varphi_t\Omega^2 + \varphi_t^3/3) + \beta_4(\varphi_t^4 + 6\varphi_t^2\Omega^2)/12$ is the instantaneous phase mismatch induced by the phase modulation of the pump $\varphi(t)$, $\Omega = \omega_p - \omega_s$ is the frequency deviation from the pump, and β_n is the nth-order dispersion coefficient. It is worth noting here that as the modulation of the signal gain is driven by the first derivative φ_t of the pump-phase modulation, the distortion induced on the signal by pump dithering will depend on the number and frequency location of the RF tones modulating the pump phase. We used the parameters: $\lambda_p = 2\pi c/\omega_p = 1563.7$ nm, zero-dispersion wavelength $\lambda_0 = 1562.9$ nm, $\beta_3 = 1.2 \times 10^{-40}$ s^3/m, and $\beta_4 = -2.85 \times 10^{-55}$ s^4/m, and a nonlinear phase shift of $\gamma PL = 3.57$ rad, yielding the maximum power gain $|\mu|^2_{max} = \cosh^2(\gamma PL) = 25$ dB, i.e., 5 dB higher than the fibre span losses to account for the insertion losses of a typical FOPA device. The corresponding FOPA design parameters are $\gamma = 10 \, (W \cdot km)^{-1}$, $L = 200$ m and $P = 1.785$ W. The inset of Fig. 1 shows the amplitude and phase spectral responses of the parametric gain as a function of the signal detuning from the pump in the absence of pump-phase modulation and their respective root-mean-square (RMS) fluctuations caused by a four-tone phase modulation (see discussion below). Whilst the amplitude fluctuation appears to be rather small, the phase fluctuation exhibits a rapid growth with increasing detuning from the pump. Therefore, we anticipated that the primary impact on the amplified signal would originate from the phase fluctuation of the gain. Within the scope of this paper, the FOPA was operated at its maximum gain ($\lambda_s = 1537.4$ nm), where the gain amplitude fluctuation is minimal.

The SBS-limited operation of the FOPA can be defined as $|\mu|^2_{max} = \cosh^2(\gamma P_{th}L)$, where P_{th} is the threshold power required for the onset of SBS, practically defined as the input pump power for which 1% of power is back scattered. Given that the Kerr-to-Brillouin figure of merit $\gamma P_{th}L$ is in the range 0.2 rad to 0.3 rad for a range of HNLFs in the 1550-nm spectral region [20,21], reaching a gain level of 25 dB requires an SBS threshold increase by a factor between 12 and 18. This can be achieved through a suitably designed multi-tone modulation of the pump phase [22]. Therefore, we considered three- and four-tone phase modulations, defined as $\varphi(t) = \sum_{j=1}^{N_t} A_{mj}\sin(\omega_{mj}t + \xi_{mj})$ ($N_t = 3$ or 4), where A_{mj}, ω_{mj} and ξ_{mj} represent the amplitude, frequency, and phase of the jth tone, respectively. The base modulation frequency ν_{m1} was set to a value higher than the Brillouin bandwidth (generally between 20 MHz and 50 MHz for typical HNLF [7]), and we selected a multiple of three spacing between successive tones to maximise the pump spectral broadening and power distribution [23]. The amplitudes and phases of the modulating tones were optimised to ensure, as much as possible, a uniform power distribution among the 3^{N_t} peaks generated across the broadened pump spectrum. This was achieved by implementing a stochastic gradient descent method in TensorFlow, which simultaneously minimised the squared differences between the individual power levels of the 3^{N_t} spectral lines and a target power level set at $1/3^{N_t}$ of the total power. Figure 2 illustrates the optimisation procedure for the four-tone phase modulation case, by showing the evolution of the mean squared error and the tone's parameters over the number of epochs (i.e., complete passes of the entire training dataset through the algorithm) and the resultant optimised power spectrum. The increase in the SBS threshold due to phase modulation can be calculated as $\Delta P_{th} = -10\log_{10}\left(\tilde{P}'_{max}/\tilde{P}_{max}\right)$, where $\tilde{P}'_{max}$ and $\tilde{P}_{max}$ represent the maximum power spectral densities over the SBS gain bandwidth with and without phase modulation, respectively [22]. The threshold enhancement factors obtained from the optimised power spectra were $\Delta P_{th} = 12.9$ dB and $\Delta P_{th} = 17.3$ dB for $N_t = 3$ and $N_t = 4$, respectively, indicating that the use of the three-tone pump dithering scheme represents a viable choice, yet it may be marginal.

Fig. 2. Evolution of (a) the mean squared error and (b, c) the tone's amplitudes and phases over the number of epochs for four-tone phase modulation. (d) Power spectrum of the pump for the optimum tone's parameters. The vertical lines delimit the spectral bandwidth $(3^4 - 1)\nu_{m1}$, and the horizontal line indicates the average power level of the 3^4 spectral peaks.
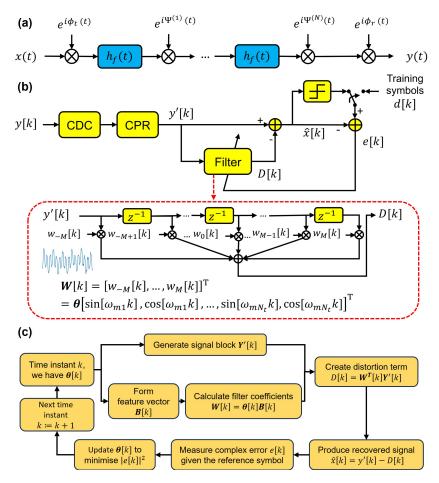
2.2. Dithering distortion compensation method

The proposed dithering distortion compensation (DDC) method was developed by back-engineering the transmission link, considering the exact interaction dynamics of the dithering-induced phase fluctuations with the chromatic dispersion. Hence, the equivalent base-band model depicted in Fig. 3(a) (the amplified spontaneous emission noise addition is not shown) was assumed, where the relationship between input $x(t)$ and output $y(t)$ signal waveforms is expressed as $y(t) = \left\{ \left[\left(\left(x(t)e^{i\phi_t(t)} * h_f(t) \right) e^{i\Psi^{(1)}(t)} \right) * \cdots * h_f(t) \right] e^{i\Psi^{(N)}(t)} \right\} e^{i\phi_r(t)}$. Here, $*$ denotes the convolution operator, $h_f(t)$ represents the linear impulse response of each fibre span, and $\phi_t(t)$, $\phi_r(t)$ are the phase noises due to nonzero line-widths of the transmitter and receiver laser sources, respectively, which were modelled as Wiener processes with increments obeying a Gaussian probability distribution [24]. The total phase noise introduced at the nth FOPA stage is given by $\Psi^{(n)}(t) = \phi_p^{(n)}(t) + \phi^{(n)}(t)$, where $\phi_p^{(n)}(t)$ is the Wiener random pump laser phase noise, and $\phi^{(n)}(t)$ represents the phase fluctuation of the FOPA's complex gain caused by the pump-phase modulation as described in Sec. 2.1. By applying linear back-propagation to the previous equation, we derived an approximate estimate of the transmitted signal $\hat{x}(t)$ from the received signal as

$$\hat{x}(t) \simeq y'(t) - \sum_{n=1}^{N} \left\{ \left[\left(y'(t) * h_f^{(n)}(t) \right) i\phi^{(n)}(t) \right] * h_e^{(n)}(t) \right\}, \qquad (2)$$

where $h_e(t)$ is the inverse response of the fibre span ($h_e(t) * h_f(t) = \delta(t)$, $\delta(\cdot)$ is the Dirac delta function), $y'(t) = e^{-i\delta\phi(t)}[y(t) * h_e^{(N)}(t)]$, and $\delta\phi(t) = \sum_n \phi_p^{(n)}(t) + \phi_t(t) + \phi_r(t)$. The responses $h_f^{(n)}(t)$ and $h_e^{(n)}(t)$ represent the accumulation by n spans. To derive Eq. (2), we assumed that the

operations of laser phase noise multiplication and channel convolution commute considering that the time scales on which phase variations due to laser phase noise take place are much longer than those associated with the dithering-induced phase noise. Moreover, we used the small signal approximation $e^{i\alpha} \simeq 1 + i\alpha$ for the phase fluctuations $\phi^{(n)}(t)$. Noticing that $y'(t)$ can be regarded as the output signal from a conventional DSP chain that includes chromatic dispersion compensation (CDC) and CPR [15], Eq. (2) evidences that the conventional DSP output differs from the transmitted signal by an additional dithering-dependent complex distortion term, which becomes more important with an increasing number of fibre spans. This is the distortion that we aim to track and compensate for.

Fig. 3. (a) Base-band equivalent of the FOPA link shown in Fig. 1(a). (b) Block diagram of the proposed DDC-enabled DSP chain. The inset shows the structure of the adaptive digital filter. (c) Flow diagram of the DDC algorithm.

Based on the aforementioned considerations, the received signal at the time instance k after matched filtering and down-sampling, $y[k]$, was first passed through conventional CDC and CPR blocks as depicted in Fig. 3(b). CDC was performed in the frequency domain by multiplying the signal spectrum by the inverse transfer function of the dispersive channel. For CPR, we used the feed-forward blind phase search (BPS) method [17], the principle of which is as follows. The signal is rotated by B test carrier phase angles, then all rotated symbols are fed into a decision circuit and the squared distances to the closest constellation points are calculated in the complex

plane. To remove noise distortions, the distances of $2K + 1$ consecutive test symbols rotated by the same carrier phase are summed up, where $2K + 1$ denotes the length of the linear filter. After filtering, the optimum phase angle is determined by searching the minimum sum of distance values, and the decoded output symbol is selected from the decision-directed symbols by a switch controlled by the index of the minimum distance sum. The output signal from the CPR stage, $y'[k]$, entered the DDC unit (Fig. 3(c)), where the distortion term described in Eq. (2) was eliminated. By approximating the channel impulse response with a finite impulse response filter, we can express this distortion term at time instance k as

$$D[k] = i \sum_{m,m'=-M/2}^{M/2} y'[k - m - m'] \sum_{n=1}^{N} \left(h_{f,m}^{(n)} \phi^{(n)}[k - m'] h_{e,m'}^{(n)} \right), \tag{3}$$

where $M/2$ is the filter delay, assumed to be independent of n and corresponding to the channel memory of the N-span link to reduce computational complexity. Equation (3) suggests that we can recreate the dithering-induced distortion by passing $y'[k]$ through an adaptive digital filter whose taps are functions of the $\phi^{(n)}[k]$ terms (inset of Fig. 3(b)). Because these taps have similar form to the first-order time derivative of the pump phase φ_t in Eq. (1), they can be predicted by fitting a parametric model with the known frequencies used for pump-phase modulation at each FOPA stage. Therefore, by using the complex least-mean-square algorithm [25], we fitted a time-varying filter $\boldsymbol{W}[k] = [w_{-M}[k], \ldots, w_M[k]]^{\mathrm{T}}$ such that $D[k] = \boldsymbol{W}^{\mathrm{T}}[k]\boldsymbol{Y}'[k]$. Here, $\boldsymbol{Y}'[k]$ represents the signal block after the conventional CDC and CPR stages at time k, containing a sufficient number of neighbouring samples. The filter was trained by updating the coefficient vector $\boldsymbol{\theta}$ in the linear regression form $\boldsymbol{W} = \boldsymbol{\theta}\boldsymbol{B}$ given the set of known frequencies $(\omega_{m1}, \ldots, \omega_{mN_t})$, where the feature vector was defined as

$$\boldsymbol{B}[k] = \left[\sin[\omega_{m1}k], \cos[\omega_{m1}k], \ldots, \sin[\omega_{mN_t}k], \cos[\omega_{mN_t}k] \right]^{\mathrm{T}}. \tag{4}$$

The transmitted signal at time k was then recovered as $\hat{x}[k] = y'[k] - \boldsymbol{W}^{\mathrm{T}}[k]\boldsymbol{Y}'[k] = y'[k] - \boldsymbol{B}^{\mathrm{T}}\boldsymbol{\theta}^{\mathrm{T}}\boldsymbol{Y}'[k]$. The update of $\boldsymbol{\theta}$ occurred at the symbol rate using the error calculated from the estimated symbol and the reference one, where the reference symbol was given from the decision-directed operation when the algorithm exited the training phase.
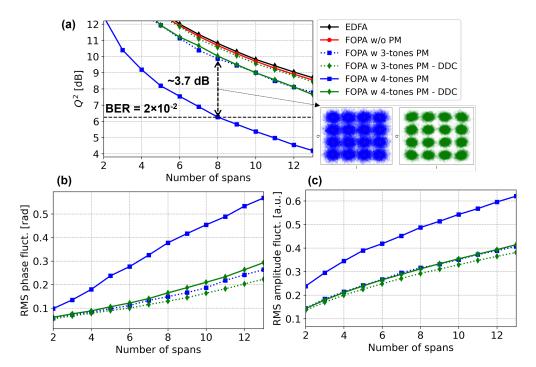
3. Results and discussion

We performed numerical simulations of the transmission of a single-polarisation 28-Gbaud 16-QAM Nyquist shaped signal with a roll-off factor of 0.1 and 8 samples per symbol over a channel consisting of $N = 13$ fibre spans. The laser line-widths were 50 kHz and 30 kHz for the transmitter and receiver units and the FOPA pumps, respectively. To avoid the signal symbols experiencing exactly the same phase distortion along the FOPA link, we included a random time shift in the pump-phase modulation sinusoidal waveform at each FOPA stage. We employed the Q^2-factor derived from the directly-counted bit-error-rate (BER) (i.e., $Q^2[\mathrm{dB}] = 20 \log(\sqrt{2}\mathrm{erfc}^{-1}(2\mathrm{BER}))$) on a total number of 10×2^{16} symbols as a system's performance metric.

Figure 4(a) shows the performance of our developed DDC algorithm as a function of the transmission length, recorded at the optimum launched signal power of 0 dBm, for the three- and four-tone pump-phase modulation schemes with a base frequency of $\nu_{m1} = 100$ MHz, i.e., with the frequency sets: [0.1, 0.3, 0.9] GHz and [0.1, 0.3, 0.9, 2.7] GHz, respectively (cf. Sec. 2.1). A test-phase resolution of $B = 32$ phase angles was used in the BPS algorithm [17]. The lengths of the BPS block filter and the DDC filter were optimised at the maximum transmission length considered (see Figs. 6(b) and 6(c)). We also included the performance curves of transmission links with in-line erbium-doped fibre amplifiers (EDFAs) and pump-dithering-free FOPAs as a reference. The latter curve was obtained under the assumption that the FOPAs were free from
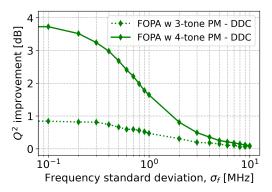
SBS, allowing them to achieve the necessary 25-dB gain without any penalties associated with this effect. It serves as an upper performance limit for our proposed DDC scheme. The amplifier's gain and noise figure were 25 dB and 4.5 dB, respectively, in all cases. The EDFA amplification obviously represents the best scenario, while the transmission scheme with dithering-free FOPAs performs marginally worse due to the accumulation of pump laser phase noise along the link. The performance difference between the three-tone and four-tone phase modulation FOPA schemes arises from the RF scheme used. The highest frequency of the four-tone scheme is significantly greater than that of its three-tone counterpart (2.7 GHz against 0.9 GHz), resulting in larger performance penalty due to increased dithering-induced distortion (see Sec. 2.1 for details). With the three-tone dithering FOPA scheme, our DDC method attains nearly 1-dB improvement in Q^2-factor over conventional DSP, paralleling the performance of the dithering-free FOPA scheme. Importantly, in the four-tone dithering case, the algorithm brings about significant performance benefits across a wide range of transmission lengths, achieving approximately 3.7-dB Q^2 improvement at a BER level of 2×10^{-2}, reached after 800-km transmission. The capability of the DDC method to mitigate both phase and amplitude distortions accrued along the transmission link is corroborated by Figs. 4(b) and 4(c). These show the evolution over the transmission length of the RMS deviations of the phases and amplitudes, respectively, of the received symbols compared to the transmitted ones, after post-processing by the conventional and DDC-enhanced DSP chains. The RMS deviation of each constellation point was calculated as $\sqrt{\frac{1}{N_s} \sum (|\hat{x}| - |x|)^2}$ for the amplitude and $\sqrt{\frac{1}{N_s} \sum (\arg(\hat{x}) - \arg(x))^2}$ for the phase, where N_s is the total number of symbols considered, and $\hat{x}$ and x are the post-processing and reference symbols, respectively (cf. Sec. 2.2). The RMS values shown in Figs. 4(b) and 4(c) are the averages over the alphabet size.

Furthermore, we evaluated the resilience of our DDC algorithm to variations in the pump dithering frequencies from their nominal values, which were employed to define the feature vector $\boldsymbol{B}$ as described in Sec. 2.2. The frequency of every phase modulation tone at each FOPA stage was sampled from a normal distribution centred around the tone's nominal frequency value and with a fixed standard deviation σ_f. Figure 5 illustrates the Q^2 improvement achieved by the DDC scheme over conventional DSP after 800-km transmission as a function of σ_f. Notably, there is no reduction in performance gain for both three- and four-tone pump-phase modulation schemes when $\sigma_f = 0.1$ MHz. However, as σ_f increases, a predictable decline in performance is observed. Yet at $\sigma_f = 1$ MHz, our DDC method can deliver roughly half of the maximum improvement realised under the ideal condition of $\sigma_f = 0$. This finding highlights a crucial design consideration for future FOPA links regarding the precision of the electronic components used for RF tone generation. In practical terms, the accuracy of these components can typically ensure that frequency fluctuations do not exceed 1 MHz, thereby sustaining the effectiveness of our DDC algorithm under realistic operational conditions.
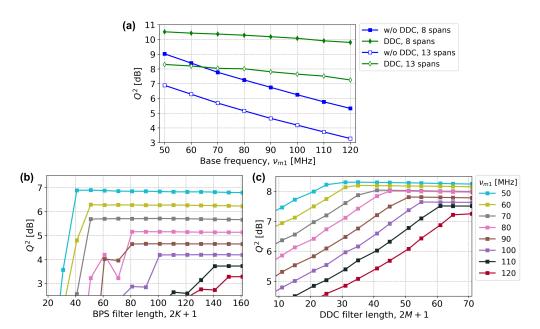
As one can observe from the results shown in Fig. 4(a), the transmission performance of the FOPA-amplified system is significantly affected by the bandwidth of the pump spectrum broadened through phase modulation, which in turn depends on the number and spacing of the dithering frequency tones. To address this aspect, we assessed the performance of our DDC method in relation to the base frequency ν_{m1} of the four-tone phase modulation scheme. The results summarised in Fig. 6(a) were obtained after 800-km and 1300-km transmissions and for ν_{m1} varied within the practical range of 50 MHz to 120 MHz. We can see that the Q^2-factor performance of the conventional DSP compensation scheme diminishes linearly and quite steeply with increasing ν_{m1}, experiencing a decline of nearly 4 dB over the surveyed ν_{m1} range. In contrast, the DDC-enhanced compensation scheme is rather robust against pump bandwidth variations, showing only about 1-dB degradation over the same ν_{m1} range. This resilience translates into a growing Q^2 gain over the conventional DSP as the pump spectrum widens.

Fig. 4. (a) Q^2-factor after conventional (CDC+CPR) (blue) and the proposed DDC-enabled (green) DSP versus number of fibre spans for three-tone (dotted) and four-tone (solid) pump-phase modulations schemes. The performance curves for in-line amplification by EDFAs (black) and pump dithering-free FOPAs (red) are also shown. The inset shows the constellation diagrams for the four-tone phase modulation without (blue) and with (green) DDC after 8 spans. (b, c) Evolution of the RMS phase and amplitude fluctuations after conventional and DDC-enabled DSP over number of fibre spans.

Fig. 5. Performance improvement of the proposed DDC scheme over conventional DSP versus standard deviation of the dithering frequencies for three-tone (dotted) and four-tone (solid) pump-phase modulation schemes after 8 fibre spans.

Fig. 6. (a) Q^2-factor after conventional (CDC+CPR) (blue) and the proposed DDC-enabled (green) DSP versus base frequency of the four-tone pump-phase modulation scheme after 8 (filled markers) and 13 (empty markers) fibre spans. (b,c) Q^2-factor after conventional and DDC-enabled DSP as a function of the BPS block filter length and the DDC filter length, respectively, for the different base frequency values used in (a).

The averaging filter length, $2K + 1$, and the number of filter taps, $2M + 1$, are key design parameters of the BPS and DDC algorithms, respectively. Figures 6(b) and 6(c) show the results of their optimisation for different values of the base frequency v_{m1} used in Fig. 6(a). The optimal values were determined as the minimum lengths beyond which no significant performance improvement was observed. The fast increase of the optimum BPS block filter length with rising v_{m1} values, as illustrated in Fig. 6(b), is attributed to the fact that the larger phase fluctuation of the FOPA's gain, and hence the increased dithering-induced phase distortion makes the estimated phase more susceptible to cycle slips – phase discontinuities of multiple of $\pi/2$, which in turn require a larger block size to reduce their occurrence. This cycle-slipping phenomenon is responsible for the fluctuating behaviour of the performance curves corresponding to high v_{m1} values (above 80 MHZ) before reaching performance saturation. Regarding the DDC algorithm (Fig. 6(c)), the longer the filter length, the stronger the ability of the algorithm to accurately model and compensate for the signal distortions. However, similarly to the BPS algorithm, once a sufficient number of neighbouring symbols are considered, this improvement saturates, indicating that excessively long filters do not yield further performance gains. The optimal length of the DDC filter increases linearly with the base frequency v_{m1} due to the larger phase fluctuations in the FOPA's gain, leading to stronger inter-symbol interference as described in Eq. (2), requiring a higher-order filter for compensation.

4.   Conclusion

We developed a new online DSP algorithm to address the phase and amplitude distortions originating from the phase modulation of the pump source and its interaction with the fibre dispersion in transmission systems with cascaded FOPAs. The algorithm, added at the end of a conventional DSP chain including CDC and CPR, effectively reconstructs these distortions

and then eliminates them from the received signal. Through detailed numerical simulations, we optimised the system's configuration for improved performance and assessed the scheme's effectiveness under non-ideal conditions. We demonstrated a notable increase in Q^2 performance, with 1-dB and 3.7-dB gains obtained for three-tone and four-tone dithering FOPA schemes, respectively, in 28-Gbaud 16-QAM long-distance transmission. This performance enhancement corresponds approximately to a 1.2-fold and 2.4-fold increase in transmission reach at a Q^2-factor of about 9 dB for the two dithering cases, respectively. We believe that our proposed scheme may become a key component of future FOPA-based transmission links, where pump dithering will be necessary to achieve high amplification gains.

References

1. M. E. Marhic, P. A. Andrekson, P. Petropoulos, *et al.*, "Fiber optical parametric amplifiers in optical communication systems," Laser Photonics Reviews **9**(1), 50–74 (2015).
2. V. Gordienko, M. F. C. Stephens, A. E. El-Taher, *et al.*, "Ultra-flat wideband single-pump raman-enhanced parametric amplification," Opt. Express **25**(5), 4810–4818 (2017).
3. T. Torounidis, P. A. Andrekson, and B.-E. Olsson, "Fiber-optical parametric amplifier with 70-dB gain," IEEE Photonics Technol. Lett. **18**(10), 1194–1196 (2006).
4. M. E. Marhic, N. Kagi, T.-K. Chiang, *et al.*, "Broadband fiber optical parametric amplifiers," Opt. Lett. **21**(8), 573–575 (1996).
5. M. Vasilyev, "Distributed phase-sensitive amplification," Opt. Express **13**(19), 7563–7571 (2005).
6. V. Gordienko, F. M. Ferreira, C. B. Gaur, *et al.*, "Looped polarization-insensitive fiber optical parametric amplifiers for broadband high gain applications," J. Lightwave Technol. **39**(19), 6045–6053 (2021).
7. J. B. Coles, B. P.-P. Kuo, N. Alic, *et al.*, "Bandwidth-efficient phase modulation techniques for stimulated Brillouin scattering suppression in fiber optic parametric amplifiers," Opt. Express **18**(17), 18138–18150 (2010).
8. Y. Aoki, K. Tajima, and I. Mito, "Input power limits of single-mode optical fibers due to stimulated Brillouin scattering in optical communication systems," J. Lightwave Technol. **6**(5), 710–719 (1988).
9. A. Mussot, A. Durécu-Legrand, E. Lantz, *et al.*, "Impact of pump phase modulation on the gain of fiber optical parametric amplifier," IEEE Photonics Technol. Lett. **16**(5), 1289–1291 (2004).
10. F. Yaman, Q. Lin, S. Radic, *et al.*, "Impact of pump-phase modulation on dual-pump fiber-optic parametric amplifiers and wavelength converters," IEEE Photonics Technol. Lett. **17**(10), 2053–2055 (2005).
11. P. Kylemark, J. Ren, Y. Myslivets, *et al.*, "Impact of pump phase-modulation on the bit-error rate in fiber-optical parametric-amplifier-based systems," IEEE Photonics Technol. Lett. **19**(1), 79–81 (2007).
12. M. Bastamova, V. Gordyenko, and A. Ellis, "Impact of pump phase modulation on fibre optical parametric amplifier performance for 16-QAM signal amplification," in *European Conference on Optical Communication (ECOC) 2022*, (Optica Publishing Group, 2022), p. Tu5.6.
13. S. Boscolo, T. T. Nguyen, A. A. I. Ali, *et al.*, "Kernel adaptive filtering-based phase noise compensation for pilot-free optical phase conjugated coherent systems," Opt. Express **30**(11), 19479–19493 (2022).
14. L. H. Nguyen, S. Boscolo, A. E. Ellis, *et al.*, "Machine learning enabled compensation of phase-to-amplitude distortion in OPC systems," in *Conference on Lasers and Electro-Optics (CLEO) 2023*, (Optica Publishing Group, 2023), p. SM3I.5.
15. S. J. Savory, "Digital filters for coherent optical receivers," Opt. Express **16**(2), 804–817 (2008).
16. I. Fatadin, D. Ives, and S. J. Savory, "Blind equalization and carrier phase recovery in a 16-QAM optical coherent system," J. Lightwave Technol. **27**(15), 3042–3049 (2009).
17. T. Pfau, S. Hoffmann, and R. Noe, "Hardware-efficient coherent digital receiver concept with feedforward carrier recovery for *M*-QAM constellations," J. Lightwave Technol. **27**(8), 989–999 (2009).
18. J. Wang and K. Petermann, "Small signal analysis for dispersive optical fiber communication systems," J. Lightwave Technol. **10**(1), 96–100 (1992).
19. M. E. Marhic, *Fiber Optical Parametric Amplifiers, Oscillators and Related Devices* (Cambridge University Press, 2007).
20. M. Deroh, J.-C. Beugnot, K. Hammani, *et al.*, "Comparative analysis of stimulated brillouin scattering at $2\,\mu$m in various infrared glass-based optical fibers," J. Opt. Soc. Am. B **37**(12), 3792–3800 (2020).

21. V. Gordienko, A. D. Szabó, M. F. C. Stephens, *et al.*, "Limits of broadband fiber optic parametric devices due to stimulated brillouin scattering," Opt. Fiber Technol. **66**, 102646 (2021).
22. J. C. Mauro, S. Raghavan, and A. B. Ruffin, "Enhanced stimulated brillouin scattering threshold through phase control of multitone phase modulation," Opt. Eng. **49**(10), 100501 (2010).
23. S. K. Korotky, P. B. Hansen, L. Eskildsen, *et al.*, "Efficient phase modulation scheme for suppressing stimulated brillouin scattering," in *Conference on Integrated Optics and Optical Fiber Communications*, vol. 1 (1995), pp. 110–111.
24. M. Lax, "Classical noise. v. noise in self-substained oscillators," Phys. Rev. **160**(2), 290–307 (1967).
25. B. Widrow, J. McCool, and M. Ball, "The complex LMS algorithm," Proc. IEEE **63**(4), 719–720 (1975).